High-Resolution Studies of Gas and Dust around Young Intermediate-Mass Stars. II. Observations of an Additional Sample of Herbig Ae Systems

Vincent Mannings

Jet Propulsion Laboratory, California Institute of Technology, MS 169-327, 4800 Oak Grove Drive, Pasadena, CA 91109

and

Anneila I. Sargent

Division of Physics, Mathematics and Astronomy, California Institute of Technology, MS 105-24, Pasadena, CA 91125

Received _____; accepted _____

ABSTRACT

In an earlier paper (Mannings & Sargent 1997) we presented evidence for disks of gas and dust associated with seven Herbig Ae stars, based on high-resolution interferometric millimeter-wave observations of continuum and molecular line emission. These systems are simultaneously high-mass analogs of the approximately solar-mass T Tauri stars and the evolutionary precursors of the prototypical main-sequence debris disk sources β Pic, α Lyr and α PsA. Here, we extend the original survey to include four additional Herbig Ae systems. We have also imaged two of the sources from Paper I at higher resolution. The new data are presented and analyzed, and are combined with the results from the earlier sample to address the properties of this class of circumstellar disk. Derived disk masses are indistinguishable from the masses of T Tauri disks. Although the combined sample is small, it seems likely that disk masses are essentially uncorrelated with stellar mass for pre-main-sequence stars of spectral type A0 and later.

Subject headings: circumstellar matter — stars: pre-main sequence

1. Introduction

Herbig Ae stars are young emission-line stars in the pre-main-sequence phase of evolution, with masses of around 2–5 $M_\odot$ (Herbig 1960; 1994). Their properties are described comprehensively in excellent reviews by Pérez & Grady (1997) and by Waters & Waelkens (1998). In common with T Tauri stars (TTs) of later spectral type, they are often found in association with nebulosity, exhibit strong metallic and Balmer spectral lines, have energetic stellar winds, often display rapid photometric and spectroscopic variability, and show continuum excesses above photospheric levels. For the TTs, continuum excesses from IR to mm wavelengths are due to thermal emission from grains in circumstellar disks (see reviews by Beckwith & Sargent 1993a; Strom, Edwards & Skrutskie 1993; Sargent 1996). In contrast, excesses observed towards Herbig Ae stars have been variously interpreted (see the review by Natta, Grinin & Mannings 2000). Explanations include emission from grains distributed in compact circumstellar disks with radii of several hundred AU (Hillenbrand et al. 1992; Natta et al. 1997), grain emission from extended envelopes with radii $\sim 10^4$ AU (Berrilli et al. 1992; Di Francesco et al. 1994; Miroshnichenko, Ivezic, & Elitzur 1997; Pezzuto, Strafella & Lorenzetti 1997), and emission from combinations of small disks and large envelopes (Natta et al. 1992; 1993). The fact that each of these geometries is equally successful in fitting the continuum spectral energy distributions of Herbig Ae stars is due principally to low angular resolution, typically 10″ to 30″ at far-IR and mm wavelengths.

In an earlier paper (Mannings & Sargent 1997; hereafter Paper I), we described the first results from our interferometric mm-wave continuum and line survey of Herbig Ae stars at resolutions of 2″ – 5″. Compact continuum emission, centered on the stars, was detected in all seven of the sources observed. Most of the dust regions were not spatially resolved, with typical upper limits to radii of about 300 AU. Estimated masses of circumstellar dust and gas were in the range 0.005 to 0.034 $M_\odot$. Molecular line emission was detected

from compact regions centered on four of the stars. In the two spatially resolved cases, HD 163296 and AB Aur, ordered gas velocity gradients were observed, consistent with Keplerian rotation in a disk. For these objects, aspherical gas morphologies, negligible optical extinctions, double-peaked mm-wave line spectra, and narrow linewidths also argues for orbiting material in disk-like configurations. By analogy, we argued that the nebular environments of the entire sample probably include substantial disk components. This was subsequently confirmed for the star MWC 480 using higher resolution measurements and kinematic modeling (Mannings, Koerner, & Sargent 1997).

The measured masses and radii for Herbig Ae disks appear remarkably similar to those for the disks surrounding the TTs (Paper I). The latter disks have masses of between 0.001 and 0.1 $M_\odot$, and outer radii typically in the range 100−500 AU (e.g. Beckwith et al. 1990, hereafter BSCG; André & Montmerle 1994; Koerner & Sargent 1995; Osterloh & Beckwith 1995; Dutrey et al. 1996; 1998; Sargent & Koerner 1999). We suggested in Paper I that, for stars of spectral type A0 and later, the bulk properties of circumstellar disks during the early stages of pre-main-sequence (hereafter pre-MS) stellar evolution may be independent of stellar mass. Here, we test this conclusion using new observations of four additional Herbig Ae stars, as well as higher frequency observations of two targets from Paper I. In §2 and §3 we describe the selection of sources, and give details of the observations. The results are presented and analyzed in §4, and discussed in §5.

2. The Sample

For the reasons given in Paper I, we continue to concentrate on stars of spectral type Ae rather than Be. The identification of Herbig Ae stars as pre-MS objects is more secure than for Herbig Be stars (cf. Calvet et al. 1994), and the cataloged Herbig Ae sources are, on average, much nearer than their Herbig Be counterparts, enabling better spatial

resolution. Perhaps most intriguing, Herbig Ae stars occupy the same range of spectral types as the main-sequence debris-disk stars α Lyr (A0V), α PsA (A3V) and β Pic (A5V) (cf. Backman & Paresce 1993; Lagrange, Backman & Artymowicz 2000), suggesting that studies of very young Ae sources will help probe the origins of these debris disks. As before, we have biased our sample towards compact, non-embedded sources by selecting only targets that exhibit mid- and far-IR continuum spectral energy distributions (SEDs $\equiv \log\nu F_\nu$ versus $\log\nu$) that decline with increasing wavelength, similar to those of optically visible TTs surrounded by inclined circumstellar disks (Adams, Lada & Shu 1987; 1988).

The Ae targets are listed in Table 1, together with coordinates, spectral types, distances, single-dish 1.3-mm flux densities, and submm spectral indices. We also tabulate total V-band extinctions, A_V. While most of these are taken from the literature, we estimate the A_V towards LkHα 259 using the cataloged spectral type, observed B and V magnitudes, the Schmidt-Kaler (1982) table of standard values of (B-V) colors, and an assumed ratio of total to selective absorption, $R = 3.1$. We also tabulate photospheric temperatures (Cohen & Kuhi 1979), together with our estimates of stellar radii, luminosities, masses and ages (see §5). As in Paper I, we have given preference to the nearer of the cataloged Herbig Ae stars (Thé, de Winter & Perez 1994) and to sources with declinations $> -25°$ for which single-dish mm-wave continuum measurements are available (Osterloh & Beckwith 1995; Sylvester et al. 1996; Mannings et al. in prep.) We have already detected MWC 758 and CQ Tau in 2.7-mm continuum emission, and unresolved ^{13}CO(1$\rightarrow$0) emission was found in association with MWC 758 (Paper I). Observations of both objects in 1.3-mm continuum and in CO(2$\rightarrow$1) line emission are reported here.

3. Observations

All measurements were made between 1996 January and 1998 January using the Owens Valley Radio Observatory (OVRO) mm-wave array at Big Pine, California. The array comprises six 10.4-m diameter telescopes. Combinations of up to three array configurations were used, with antenna spacings ranging from 15 to 200 m E−W and from 15 to 220 m N−S. The sizes of the naturally-weighted synthesized beams were $4'' - 5''$ (FWHM) at $\lambda \approx 3$ mm, and $2''$ (FWHM) at $\lambda \approx 1$ mm. Cryogenically cooled SIS receivers on each telescope produced average single sideband system temperatures of 1000 and 1550 K at the frequencies of the CO(1→0) and CO(2→1) lines, respectively. For the CO(1→0) observations of MWC 614, HD 34282, MacC H12, and LKHα 259, the digital correlator was configured to provide two bands of Hanning-smoothed channels, 64×0.5 MHz and 64×0.125 MHz, with velocity resolutions of 1.30 and 0.33 km s^{-1}, respectively. High-resolution CO(2→1) measurements of MWC 758 and CQ Tau used bands of 64×0.125 MHz and 64×0.5 MHz, with corresponding velocity resolutions of 0.16 and 0.65 km s^{-1}. Where there was no prior knowledge of systemic velocities, we centered spectrometer bands at $v_{\rm LSR} = 0$. At all frequencies, simultaneous continuum measurements were made using an analog correlator of bandwidth 1 GHz.

Calibration of visibility phases and amplitudes was achieved with observations of quasars, typically at intervals of 20 minutes. The quasar 0528+134 was used for phase and amplitude calibration of MWC 758 and CQ Tau; 0133+476 and 0224+671 were used for both MacC H12 and LkHα 259; for MWC 614, 1749+096 and 2023+336 were used, while 0420-014 and 0607-157 were used for HD 34282. Measurements of 3C 273, 3C 345 and 3C 454.3 were made to calibrate the spectrometer passbands, and observations of Uranus and Neptune provided an absolute flux density scale. Calibration was carried out using the in-house software package, MMA (Scoville et al. 1993). Continuum and spectral line maps

were generated and CLEANed using the NRAO AIPS package. Uncertainties in fluxes and source positions are estimated to be about 20% and 0″.5, respectively. The average 1σ rms noise levels on the continuum maps are 2.1 and 7.3 mJy beam^{-1} at λ = 2.6 and 1.3 mm, respectively. For the spectral line channels, the average 1σ rms is 0.103 Jy beam^{-1} (Δv = 0.65 km s^{-1}) at CO(2→1), and 0.124 Jy beam^{-1} (Δv = 1.3 km s^{-1}) at CO(1→0).

4. Results and Analysis

4.1. Continuum Emission

Unresolved continuum emission was detected from all targets except the distant source LkHα 259. Contour maps are presented in Fig 1, and measured flux densities are given in Table 2. Column (4) of Table 2 lists upper limits to radii, corresponding to half the FWHM of the minor axes of the synthesized beams. Assuming the source distances in Table 1, these limits range from 80 AU for CQ Tau to 1625 AU for MacC H12.

Within the errors, the continuum peak and the stellar position are spatially coincident for each Herbig Ae system. We therefore assume that all compact continuum sources in our sample are centered upon the target stars.

Our measured flux densities provide rough estimates of the masses of circumstellar material, assuming that emission at mm wavelengths is optically thin. Then,

$$M = \frac{F_\nu d^2}{\kappa_\nu B_\nu(T)}, \tag{1}$$

where d is the distance to the source, and κ is the mass opacity coefficient at frequency ν. Assuming a gas-to-dust ratio of 100, by mass, and $\kappa_{\lambda=0.25\mathrm{mm}} = 0.1$ cm^2 g^{-1}, we extrapolate to mm wavelengths using $\kappa \propto \nu^\beta$ with $\beta = 1$ (cf. Beckwith & Sargent 1991; Mannings &

Emerson 1994). The same values of opacity and gas-to-dust ratio were used by BSCG, Osterloh & Beckwith (1995), and André & Montmerle (1994) to derive the masses of circumstellar material in T Tauri systems, permitting a direct comparison with the masses derived here (§5). Adopting for each source a characteristic temperature of 40 K (again, see Beckwith & Sargent 1991; Mannings & Emerson 1994), we obtain the mass estimates given in column (5) of Table 2, and they range from 0.009 $M_\odot$ (CQ Tau) to 0.234 $M_\odot$ (MacC H12). Note that, for $\beta = 1$ and $\lambda = 3$ mm, $\kappa = 0.0083$ cm^2 g^{-1}, which is significantly higher than suggested by the results of Pollack et al. (1994). The mass estimates presented here may therefore be conservatively low, probably by a factor of 3–4.

Using these measurements of mass and radius, we can compute values of A_V along the line of sight through a given continuum source to the central star, as in Paper I. In Table 2 we list A_V for uniform density and freely-falling spherical envelopes. The extinctions range from around 20 to 250 magnitudes for the physically unlikely case of uniform density envelopes, and from 400 to >1000 magnitudes for envelopes in free-fall. Such values are far in excess of extinctions implied by the spectral types and observed colors, which are in the range 0.2 to 5.6 (§2 and Table 1). This suggests that most of the observed dust is distributed aspherically about the Herbig Ae stars, perhaps in the form of disks.

4.2. Molecular line emission

Molecular line emission was detected in three of the six sources observed: MWC 758, MacC H12, and CQ Tau. Spatially integrated line spectra are plotted against velocity in Fig 2. Table 3 lists observed systemic velocities (v_0), velocity ranges (Δv) over which emission appears above the 3σ level, and integrated intensities, $\int S_\nu dv$. Figure 3 displays contour maps of line emission integrated over the full velocity ranges, together with corresponding maps of the spatial distribution of intensity-weighted mean velocities across

each of the gas structures. MWC 758 and MacC H12 are clearly spatially resolved, but are not circularly symmetric. CQ Tau is not spatially resolved. For all three sources, the separation of the stellar position and the centroid of the gas structure is much less than half the beam size. As for the dust regions, we assume that the molecular line emission arises in gas that is associated with and centered upon the stars.

Elliptical Gaussian brightness profiles were fitted to the maps of integrated intensity and then deconvolved from the Gaussian beams to obtain the radii at half-maximum intensity listed in column (6) of Table 3. The semi-major axes are 245 AU along PA = $116°^{+6}_{-5}$ and 4250 AU along PA = $136°^{+3}_{-3}$ for MWC 758 and MacC H12, respectively, assuming the distances listed in Table 1. For CQ Tau, we obtain an upper limit of 85 AU for the radius of the gas structure. The semi-minor axis of the molecular emission from MWC 758 is 170 AU. From the aspect ratio, we obtain an inclination angle of $i \approx \cos^{-1}\,(^{170}/_{245}) \approx 46°$ (where 0° is face-on). MacC H12 has a semi-minor axis of 2870 AU, suggesting an inclination angle $i \approx 48°$.

The right-hand panels of Fig. 3 show greyscale maps of the spatial distribution of intensity-weighted mean velocities across each of the three gas structures — i.e. first-moment maps with respect to gas velocity. Such maps are crude in the sense that at each point we characterize the full range of gas velocities along the line-of-sight by just one value, but they provide a useful probe for ordered bulk gas motions if the major axis can be identified unambiguously (cf. Koerner & Sargent 1995; Koerner 1997). Our first-moment maps indicate ordered velocity gradients in all three cases. For both MWC 758 and CQ Tau, blue-shifted emission is confined to the east of the star, while red-shifted emission is found only to the west. The above-mentioned Gaussian fit to the zeroth-moment map of CQ Tau is dominated by the bright and unresolved core of the emission profile but, in the first-moment map, the emission is marginally resolved along the major axis. The upper

limit of 85 AU for the radius is probably close to the actual value. The spatial compactness, narrow linewidths (see also below) and the ordered velocity gradients along the major axes strongly support the hypothesis that the material around MWC 758 and CQ Tau is rotating in Keplerian orbits. By contrast, MacC H12 has an irregular shape, and the gradient is orthogonal to the apparent major axis. This source is discussed further in §5.

The CO line profiles for MWC 758 and CQ Tau are a particularly useful diagnostic. There is no evidence of extended velocity wings characteristic of outflow motions (cf. Bachiller 1996). Although the two remaining kinematic options, infall and rotation, should generate double-peaked lines (e.g. Beckwith & Sargent 1993b), neither MWC 758 nor CQ Tau display this feature, presumably due to insufficient velocity resolution. However, the width of the line for MWC 758 can help discriminate between infall and rotation. Using the stellar mass given in Table 1 and the disk radius and inclination angle from Table 3, the angle-adjusted Keplerian velocity, $(GM_*/R_D)^{0.5}$, is v_{Kep}=1.9 km/s. This is just a little higher than half the line width, or 1.3 km/s, for the spectrum shown in Fig 2, and it is substantially less than the theoretical infall velocity $v_{inf}=\sqrt{2}v_{Kep}$=2.7 km/s. Keeping in mind that these calculations are rough, and that they involve a mix of quantities derived from a spectrum, a map and the H-R diagram (§5), the fact that $v_{obs} < v_{Kep} < v_{inf}$ argues for gas moving in Keplerian orbits around MWC 758. These arguments cannot, however, be applied to CQ Tau, where the emission is spatially unresolved and the inclination angle is unknown.

Total masses of circumstellar gas can be determined from the observed velocity-integrated emission, $\int S_\nu dv$, and the following conversions (cf. Scoville et al. 1986) for CO(1→0) and CO(2→1), respectively:

$$M_{H_2}(M_\odot) = 2.19 \times 10^{-5} \frac{(T_x + 0.93)}{e^{-5.59/T_x}} \frac{\tau_{CO}}{(1 - e^{-\tau})}$$

$$\times d_{\rm kpc}^2 \int S_\nu {\rm d}v \qquad (2)$$

$$M_{\rm H_2}({\rm M}_\odot) = 1.42 \times 10^{-10} \frac{(T_{\rm x} + 0.93)}{{\rm e}^{-16.76/T_{\rm x}}} \frac{\tau_{\rm CO}}{(1 - {\rm e}^{-\tau})} \times \frac{d_{\rm kpc}^2}{{\rm X_{CO}}} \int S_\nu {\rm d}v \qquad (3)$$

where S_ν is in units of Jy, v is in km s^{-1}, $T_{\rm x}$ is excitation temperature, τ is optical depth in the given line and X is fractional abundance, relative to molecular hydrogen. In the optically thin limit, the mass is straightforwardly calculable; here, only lower limits to masses of molecular hydrogen can be computed. These are presented in column (9) of Table 3, where we have assumed for all four sources an excitation temperature of 40 K. The fractional abundance of CO is taken to be 10^{-4}.

The computed gas masses in Table 3 disagree, sometimes by orders of magnitude, with those determined using our continuum flux densities (see Table 2). The ratios of total masses derived from continuum and spectral line measurements are 378 for MWC 758, 6 for MacC H12, and 344 for CQ Tau. Similar discrepancies were found for Herbig Ae sources in Paper I and for T Tauri systems (Dutrey, Guilloteau & Simon 1994; Koerner & Sargent 1995; Dutrey et al. 1996). Suggested causes are CO depletion onto grains at low temperatures, or contributions to observed line emission from optically thick regions of molecular gas (Dutrey et al. 1996; Sargent 1996 and references therein). Mass determinations based on observations using optically thin line emission from other CO isotopomers or other molecules are probably necessary to clarify this issue. In the meantime we assume that the continuum fluxes, which are very likely optically thin, provide more reliable estimates of the masses of circumstellar material despite uncertainties in the value of κ_ν.

5. Discussion

The observations described here identify compact sources of millimeter-wave emission centered upon most of the Herbig Ae stars in our sample. As in Paper I, we see directly that continuum and, in several cases, molecular line emission arises from material located typically within a few hundred AU of each target. Estimated masses of circumstellar gas and dust, based on the continuum measurements, would lead to V-band extinctions of up to 10^3 magnitudes and more if the circumstellar material is distributed spherically. Observed values of A_V are in the range 0.2 to 5.5 (Table 1), suggesting relatively flattened and inclined sources of emission. Elongated morphology is in fact seen in the MWC 758 image; both the CO linewidth and a velocity gradient along the major axis also argue for the presence of a rotating disk. Evidence for Keplerian gas motions is less compelling for CQ Tau, but the compactness of the source in continuum and CO line emission ($r \lesssim 100$ AU) is consistent with expectations for a rotating disk, such as those seen in other Herbig Ae and T Tauri systems.

The properties of the circumstellar material in MacC H12 are very different. Our CO map reveals an aspherical source of size 4250 $\times$ 2870 AU, an order of magnitude greater than usual for Herbig Ae and T Tauri systems, while the continuum flux implies a mass about 10 times higher (cf. Table 4). The orientation of the velocity gradient along the minor axis in the first-moment map of Fig 3 suggests that MacC H12 is a very young star, perhaps still embedded within an infalling envelope (cf. Hayashi, Ohashi & Miyama 1993). In this case, we anticipate a Class I SED (Lada 1987), rising sharply at far-IR wavelengths. However, the IR–mm SED of MacC H12 (Pezzuto et al. 1997) strongly resembles the Class II SEDs that are typical of T Tauri star/disk systems, where emission falls off with increasing wavelength. Indeed, it is very similar to the IR–mm SEDs of the star/disk Ae systems AB Aur and HD 163296 (Mannings 1994; Paper I). Additionally, if embedded (and

therefore presumably young), we would expect MacC H12 to be on or close to the Stahler birthline on the Hertzsprung–Russell diagram. We show the locations[1] of all our target stars on the H–R plane in Fig. 4. MacC H12 appears far below the birthline, with an age of about 3 Myr. It is unlikely that a star of this age would be accompanied by the extended structure revealed in Fig. 3. Possible explanations include source confusion (the mm-wave source is not associated with the cataloged Ae star MacC H12) or incorrect spectral type and/or A_V, each of which would invalidate the position plotted on the H–R diagram. Observations with greater sensitivity and better resolution are clearly required to search for multiple sources and to examine gas kinematics in more detail.

All objects in our present sample are plotted as filled circles in Fig. 4. Sources from Paper I are represented by open circles. As already noted by van den Ancker, de Winter & Tjin A Djie (1998), HD 34282 appears well below the main sequence. This is probably due to a mis-classification of spectral type or to an error in the distance determination. Stellar masses and ages inferred from Fig. 4 range from 1.5 $M_\odot$ (CQ Tau) to 4 $M_\odot$ (MWC 614),

---

[1]Spectral types were converted to photospheric effective temperatures using the the results of Cohen & Kuhi (1979). Uncertainties in $T_{\rm eff}$ were estimated from the range of spectral types claimed in the literature for each Ae star. Stellar radii and luminosities were derived by fitting dereddened optical magnitudes. Uncertainties in luminosities were estimated using both the range of spectral types and the known optical variability (Thé et al. 1994). Theoretical pre-MS mass tracks and isochrones plotted on the H–R diagram in Fig. 4 are from digital files kindly made available by Francesco Palla (see also Palla & Stahler 1993). In Paper I we used mass tracks by D'Antona & Mazzitelli (1994), which include stars up to masses of 2.5 $M_\odot$. The mass tracks used here extend to masses of 6 $M_\odot$ and are needed in order to obtain masses for our full sample of stars. Our estimates of stellar radii, luminosities, masses and ages are given in Table 1.

and from 0.3 Myr (LkHα 259 and MWC 614) to 10 Myr (CQ Tau), respectively.

Within the set of sources discussed here and in Paper I, can we discern any trends of disk properties with age and stellar mass? Figure 5 shows plots of circumstellar mass and source radius as functions of stellar age and mass[2]. Because of the uncertainties, we exclude MacC H12. No correlations between circumstellar mass and stellar age, or between circumstellar mass and stellar mass, are evident in Fig. 5(a) and Fig. 5(b). The same conclusion was drawn for TTs disks by BSCG for the same range of ages. The mass range for Ae disks in the present work is within the mass range of Paper I, and this range is indistinguishable from the masses of TTs disks (Table 4). Disk masses may therefore be independent of stellar mass from $M_* \approx 0.5$ to 4 $M_\odot$. Disk radii extend across a range similar to that measured for TTs disks (Table 4). In Fig. 5(c), disk radius appears to decrease with age, but the trend relies heavily upon the first and last data-points (AB Aur and CQ Tau, respectively). The radius of CQ Tau's disk is by far the smallest of any of the Ae systems imaged to date, and is also smaller than any of the TTs disks (cf. Koerner & Sargent 1995, and Sargent & Koerner 1999). While CQ Tau is the oldest Ae star in our sample, we are reluctant to attribute the small size to disk evolution, given the limited sample here. The disk may simply be at the low end of the range of masses and radii exhibited by Ae disks. Likewise, the sample size prevents any firm conclusion to be drawn from Fig. 5(d), where there appears to be a correlation between Ae disk radii and stellar masses.

---

[2]In Paper I we used the mass tracks and isochrones of D'Antona & Mazzitelli (1994). For consistency within the combined sample, we use the masses and ages of the Paper I sample implied by the tracks of Palla & Stahler (1993) plotted in Fig. 4. They are: 2.5 $M_\odot$ and 3 Myr (AB Aur), 2.3 $M_\odot$ and 4 Myr (HD 163296), 2.2 $M_\odot$ and 4 Myr (MWC 863), 2.0 $M_\odot$ and 7 Myr (HD 245185), and 2.0 $M_\odot$ and 6 Myr (MWC 480). These values are in fact very similar to those deduced in Paper I.

Note that, when interpreting Fig. 5, there are two caveats: first, the disk masses are derived from spatially unresolved continuum measurements, while the radii are from the CO images. However, the two derived quantities essentially characterize the same source: since the density profiles rise sharply with decreasing radius, most of a disk's mass is contained within the unresolved region measured by continuum observations. At the same time, dust and gas are spatially coincident out to the CO radius, although the emission of the dust falls off more rapidly. Second, from the perspective of disk properties, stellar age and stellar mass are not necessarily independent parameters. Given a sufficiently large sample of stars with a good spread in both age and mass, it should be possible to explore the variation of disk mass and disk radius with respect to, separately, age and stellar mass. We have therefore used our small sample here to make only a first step in searching for trends.

6. Summary and Conclusions

As a follow-up to our study of seven Herbig Ae systems (Paper I), we have imaged four additional Ae sources at high spatial resolution and mapped two of the original seven sources, MWC 758 and CQ Tau, in the 1.3-mm band to achieve higher resolution. Thermal continuum emission from dust was detected from all except one source, LkHα 259, which is very distant. Molecular line emission was measured toward MacC H12, as well as from MWC 758 and CQ Tau. All detected dust and gas regions are centered on the target stars. The dust regions are not resolved and we place upper limits to radii ranging from 80 AU for the nearest source, CQ Tau, to 1625 AU for MacC H12. Continuum fluxes imply masses of dust and gas in the range 0.009 to 0.021 $M_\odot$ for, in order of increasing mass, CQ Tau, MWC 758, MWC 614, and HD 34282.

Molecular line emission from MWC 758 is spatially resolved and elongated, with a semi-major axis of 245 AU. The aspect ratio yields an inclination angle of 46°. A velocity

gradient along the major axis is observed, consistent with the presence of a rotating disk of circumstellar material. The CO map for CQ Tau is dominated by a bright and unresolved central core of emission with radius $\leq$ 85 AU. There is weak evidence for a velocity gradient. We suggest that CQ Tau, like MWC 758, is surrounded by a Keplerian disk, and that the circumstellar environments of MWC 614 and HD 34282 include substantial disk components. Indeed, visual extinctions computed for spherical distributions of material with the above radii and masses are much higher than the actual extinctions observed toward each of the stars in our sample. Note also that single-dish CO(3$\rightarrow$2) measurements of HD 34282 (Greaves, Mannings & Holland 1999), display the narrow and double-peaked profile characteristic of gas that is rotating or infalling in a plane. Higher-resolution observations of HD 34282 in CO(2$\rightarrow$1) and 1.3-mm continuum emission should clarify this situation. The gas and dust region nominally associated with the distant star MacC H12 is an order of magnitude greater in size and mass than the disks encircling MWC 758 and CQ Tau, and we propose that the central star is relatively young and still embedded within an envelope. The star itself may not be the cataloged Ae star MacC H12.

Combining the new results with those of Paper I provides a sample of some 11 Herbig Ae systems. Excluding MacC H12, they range in age from 0.3 to 10 Myr, with stellar masses from 1.5 to 4 $M_\odot$. Although the sample is small, and biased by the selection criteria, it seems that disk masses are uncorrelated with both stellar age and with stellar mass, similar to TTs aged 10 Myr and less. The Herbig Ae disk masses are indistinguishable from TTs disk masses, so that disk masses appear to be independent of the masses of the central stars across the range $0.5 \lesssim M_*/M_\odot \lesssim 4$. For the subset of 5 sources with spatially resolved gas regions, AB Aur, HD 163296, MWC 480, MWC 758 and CQ Tau, there is some indication of a decrease of disk radius with age, and an increase of radius with stellar mass. However, these trends remain to be confirmed with a larger and better-populated sample of stellar ages and masses.

The Owens Valley millimeter-wave array is supported by NSF grant AST-96-13717. Research at Owens Valley on young star and disk systems is also supported by the *Norris Planetary Origins Project*, for which we are very grateful. We are also grateful to NASA's *Origins of Solar Systems* program, which provides funding through grant NAGW-4559. An anonymous referee is thanked for useful suggestions. We thank Francesco Palla for kindly providing pre-MS mass tracks and isochrones. Jane Greaves and Roger Sylvester are thanked for useful discussion and comments. This research has made use of NASA's Astrophysics Data System Abstract Service, together with the SIMBAD database operated at CDS, Strasbourg, France.

REFERENCES

Adams, F. C., Lada, C. J., & Shu, F. H. 1987, ApJ, 312, 788

Adams, F. C., Lada, C. J., & Shu, F. H. 1988, ApJ, 326, 865

André, P., & Montmerle, Th. 1994, ApJ, 420, 837

Backman, D. E., & Paresce, F. 1993, in Protostars and Planets III, eds. E. H. Levy & J. I. Lunine, (Tucson:University of Arizona Press), 1253

Bachiller, R. ARA&A, 34, 111

Beckwith, S. V. W., & Sargent, A. I. 1991, ApJ, 381, 250

Beckwith, S. V. W., & Sargent, A. I. 1993a, in Protostars and Planets III, eds. E. H. Levy & J. I. Lunine (Tucson:University of Arizona Press), 521

Beckwith, S. V. W., & Sargent, A. I. 1993b, ApJ, 402, 280

Beckwith, S. V. W., Sargent, A. I., Chini, R. S., & Güsten, R. 1990, AJ, 99, 924 (BSCG)

Berrilli, F., Corciulo, G., Ingrosso, G., Lorenzetti, D., Nisini, B., & Strafella, F. 1992, ApJ, 398, 254

Calvet, N., Hartmann, L., Kenyon, S. J., & Whitney, B. 1994, PASP Conf. Series, 62, 207

Cohen, M. & Kuhi, L. V. 1979, ApJS, 41, 743

D'Antona, F., & Mazzitelli, I. 1994, ApJS, 90, 467

Di Francesco, J., Evans, N. J., Harvey, P. M., Mundy, L. G., & Butner, H. M. 1994, ApJ, 432, 710

Dutrey, A., Guilloteau, S., & Simon, M. 1994, A&A, 286, 149

Dutrey, A., Guilloteau, S., Duvert, G., Prato, G., Simon, M., Schuster, K., & Ménard, F. 1996, A&A, 309, 493

Dutrey, A., Guilloteau, S., Prato, L, Simon, M., Duvert, G., Schuster, K., & Ménard, F. 1998, A&A, 338, L63

ESA 1997, The Hipparcos and Tycho Catalogues, ESA SP-1200

Greaves, J. S., Mannings, V., & Holland, W. S. 1999, Icarus, in press

Hayashi, M., Ohashi, N., and Miyama, S. M. 1993, ApJ, 418, L71

Herbig, G. H. 1960, ApJS, 4, 337

Herbig, G. H. 1994, PASP Conf. Series, 62, 3

Herbig, G. H., & Bell, K. R. 1988, Lick Obs. Bull. No. 1111

Hillenbrand, L. A., Strom, S. E., Vrba, F. J., & Keene, J. 1992, ApJ, 397, 613

Koerner, D. W. 1997, in CO: 25 Years of Millimeter-Wave Spectroscopy, proceedings to IAU Symposium #170, eds. W. B. Latter et al. (Kluwer, Dordrecht), 162-164

Koerner, D. W., & Sargent, A. I. 1995, AJ, 109, 2138

Lada, C. J. 1987, in IAU Symp. 115, Star Forming Regions, ed. M. Peimbert & J. Jugaku (Dordrecht: Kluwer), 1

Lagrange, A.-M., Backman, D., & Artymowicz, P. 2000, in Protostars and Planets IV, ed. V. Mannings, A. P. Boss & S. S. Russell, (Tucson: University of Arizona Press), in press

Levreault, R. M. 1988, ApJS, 67, 283

Mannings, V. 1994, MNRAS, 271, 587

Mannings, V., & Emerson, J. P. 1994, MNRAS, 267, 361

Mannings, V., & Sargent, A. I. 1997, ApJ, 490, 792 (Paper I)

Mannings, V., Koerner, D. W., & Sargent, A. I. 1997, Nature, 388, 555

Miroshnichenko, A., Ivezic, Z., & Elitzur, M. 1997, ApJ, 475, L41

Natta, A., Grinin, V. P., & Mannings, V. 2000, in Protostars and Planets IV, ed. V. Mannings, A. P. Boss & S. S. Russell, (Tucson: University of Arizona Press), in press

Natta, A., Palla, F., Butner, H. M., Evans, N. J., & Harvey, P. M 1992, ApJ, 391, 805

Natta, A., Palla, F., Butner, H. M., Evans, N. J., & Harvey, P. M. 1993, ApJ, 406, 674

Natta, A., Grinin, V. P., Mannings, V., & Ungerechts, H. 1997, ApJ, 491, 885

Osterloh, M., & Beckwith, S. V. W. 1995, ApJ, 439, 288

Palla, F., & Stahler, S. W. 1993, ApJ, 418, 414

Pérez, M. R., & Grady, C. A. 1997, Sp. Sci. Rev., 82, 407

Pezzuto, S., Strafella, F., & Lorenzetti, D. 1997, ApJ, 485, 290

Pollack, J. B., Hollenbach, D., Beckwith, S. V. W., Simonelli, D. P., & Fong, W. 1994, ApJ, 421, 615

Sargent, A. I. 1996, in Disks & Outflows around Young Stars, eds. S. V. W. Beckwith, J. Staude, A. Quetz, & A. Natta (Berlin, Springer-Verlag), 1

Sargent, A. I., & Koerner, D. W. 1999, in preparation

Scoville, N. Z., Sargent, A. I., Sanders, D. B., Claussen, M. J., Masson, C. R., Lo, K. Y., & Phillips, T. G. 1986, ApJ, 303, 416

Scoville, N. Z., Carlstrom, J. E., Chandler, C. J., Phillips, J. A., Scott, S.L., Tilanus, R. P. J., and Wang, Z. 1993, PASP, 105, 1482

Schmidt-Kaler, Th. 1982, in K. Schaifers & H. H. Voigt, eds, Landolt-Börnstein, Numerical Data and Functional Relationships in Science and Technology, Group VI, Astronomy, Astrophysics and Space Research, Vol. 2b (Berlin:Springer-Verlag), p. 15

Strom, S. E., Edwards, S. & Skrutskie, M. F. 1993, in Protostars & Planets III, eds. E. H. Levy & J. I. Lunine, (Tucson: University of Arizona Press), 837

Sylvester, R. J., Skinner, C. J., Barlow, M. J., & Mannings, V. 1996, MNRAS, 279, 915

Thé, P. S., de Winter, D., & Pérez, M. R. 1994, A&AS, 104, 315

van den Ancker, M. E., de Winter, D., & Tjin A Dje, H. R. E. 1998, A&A, 330, 145

Waters, L. B. F. M., & Waelkens, C. 1998, ARA&A, 36, 233

This manuscript was prepared with the AAS LaTeX macros v4.0.

Fig. 1.— Contour plots of continuum emission. The centers of the maps correspond to the phase centers of the fields during the measurements with the array which, in turn, are located at the stellar positions precessed from their equinox 1950.0 equatorial coordinates. The latter were taken from the Hipparcos Input Catalog for MWC 614 and HD 34282, and include proper motions to the epoch of the OVRO observations. Phase center coordinates for MWC 758 and CQ Tau were obtained from the SAO catalog. For MacC H12 we used the catalog of Herbig & Bell (1988). Offsets in units of arc seconds from the phase centers are indicated along the horizontal and vertical axes. Black asterisks represent stellar positions, corresponding simply to the phase center for MacC H12, and to newly available coordinates from the Hipparcos & Tycho Catalogues (ESA 1997) for MWC 614, HD 34282, MWC 758 and CQ Tau (including new values for proper motions). Ellipses in the upper left corners of the panels indicate position angles and FWHM of the synthesized beams. Contours on all maps begin at 3σ; the 1σ rms noise and contour interval are, respectively, 1.2 mJy beam^{-1} and 0.5σ for MWC 614 (λ=2.6 mm), 5.3 mJy beam^{-1} and 1σ for MWC 614 (λ=1.3 mm) , 3.5 mJy beam^{-1} and 0.5σ for HD 34282, 4.7 mJy beam^{-1} and 2σ for MWC 758, 1.5 mJy beam^{-1} and 0.5σ for MacC H12, and 12.0 mJy beam^{-1} and 2σ for CQ Tau. Flux densities are listed in Table 2.

Fig. 2.— Spatially integrated spectra. MWC 758 and CQ Tau were observed in CO(2→1), while MacC H12 was mapped in CO(1→0). The flux density scale, in Jy, ranges by about one order of magnitude to allow easy comparison of the lineshapes for the three Herbig Ae systems.

Fig. 3.— Molecular line emission maps. The panels show show contours of velocity-integrated intensities (*left*) and greyscales of intensity-weighted mean velocities (*right*). Offsets in arc seconds from the phase centers are indicated along the horizontal and vertical axes. Star symbols represent stellar positions (see caption to Fig. 1). The FWHM and orientations of the synthesized beams are indicated in the upper left corner of each map. Contours begin at a level of 3σ; intensities are listed in Table 3.

Fig. 4.— H-R diagram, with stellar temperatures and luminosities for the present sample taken from Table 1; see also §5. Mass tracks and isochrones are from F. Palla (private communication; see Palla & Stahler 1993). ZAMS stellar masses are indicated along the main sequence in units of $M_{\odot}$.

Fig. 5.— Disk masses and radii plotted against stellar ages and stellar masses. See discussion in §5.

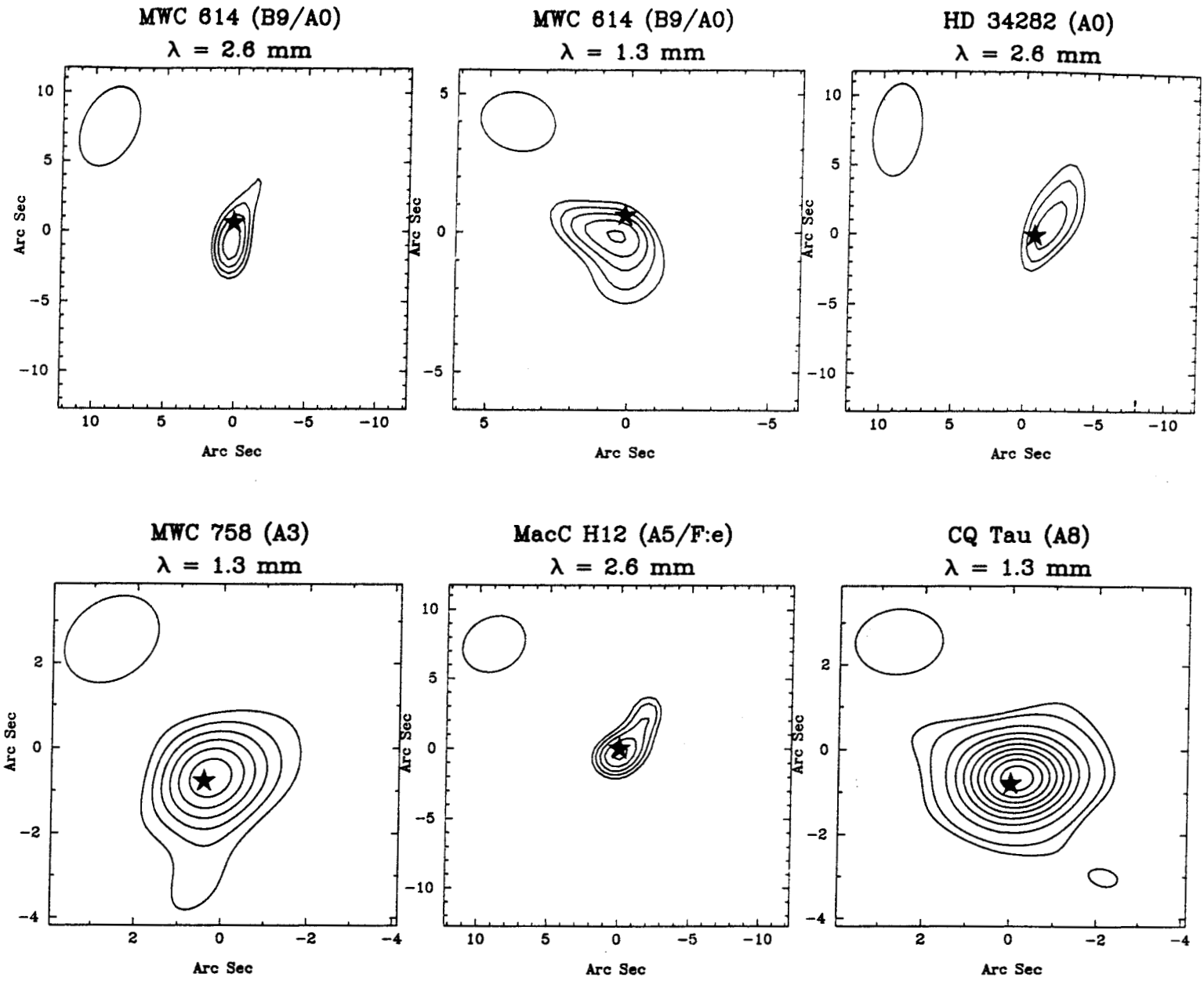
MWC 614 (B9/A0)
λ = 2.6 mm
MWC 614 (B9/A0)
λ = 1.3 mm
HD 34282 (A0)
λ = 2.6 mm
MWC 758 (A3)
λ = 1.3 mm
MacC H12 (A5/F:e)
λ = 2.6 mm
CQ Tau (A8)
λ = 1.3 mm
Arc Sec

Fig. 1

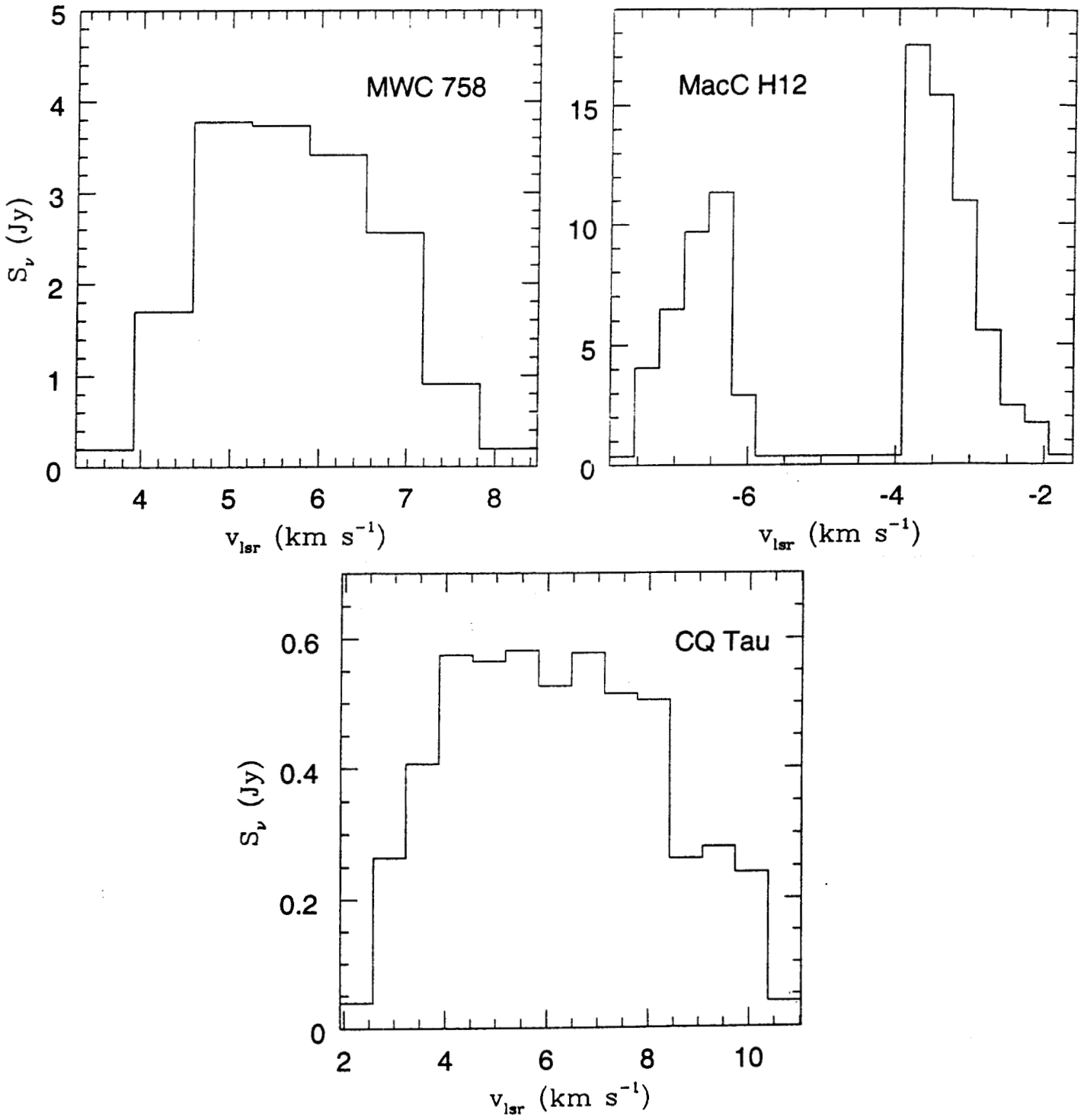

Fig. 2

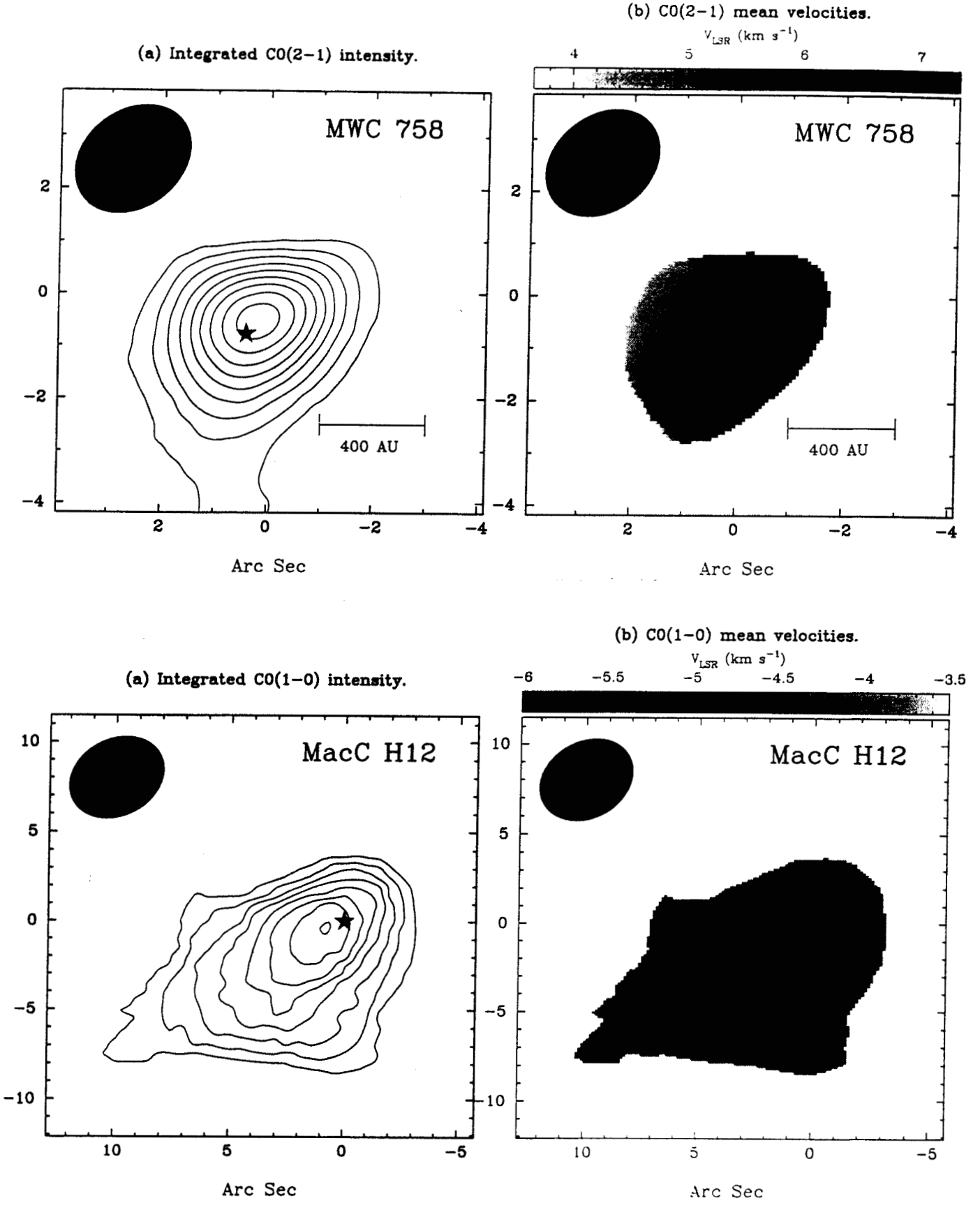
(a) Integrated CO(2−1) intensity.
(b) CO(2−1) mean velocities.
V_{LSR} (km s^{-1})
4
5
6
7
MWC 758
MWC 758
400 AU
400 AU
2
0
−2
−4
Arc Sec
Arc Sec
(a) Integrated CO(1−0) intensity.
(b) CO(1−0) mean velocities.
V_{LSR} (km s^{-1})
−6
−5.5
−5
−4.5
−4
−3.5
MacC H12
MacC H12
10
5
0
−5
−10
Arc Sec
Arc Sec

Fig. 3

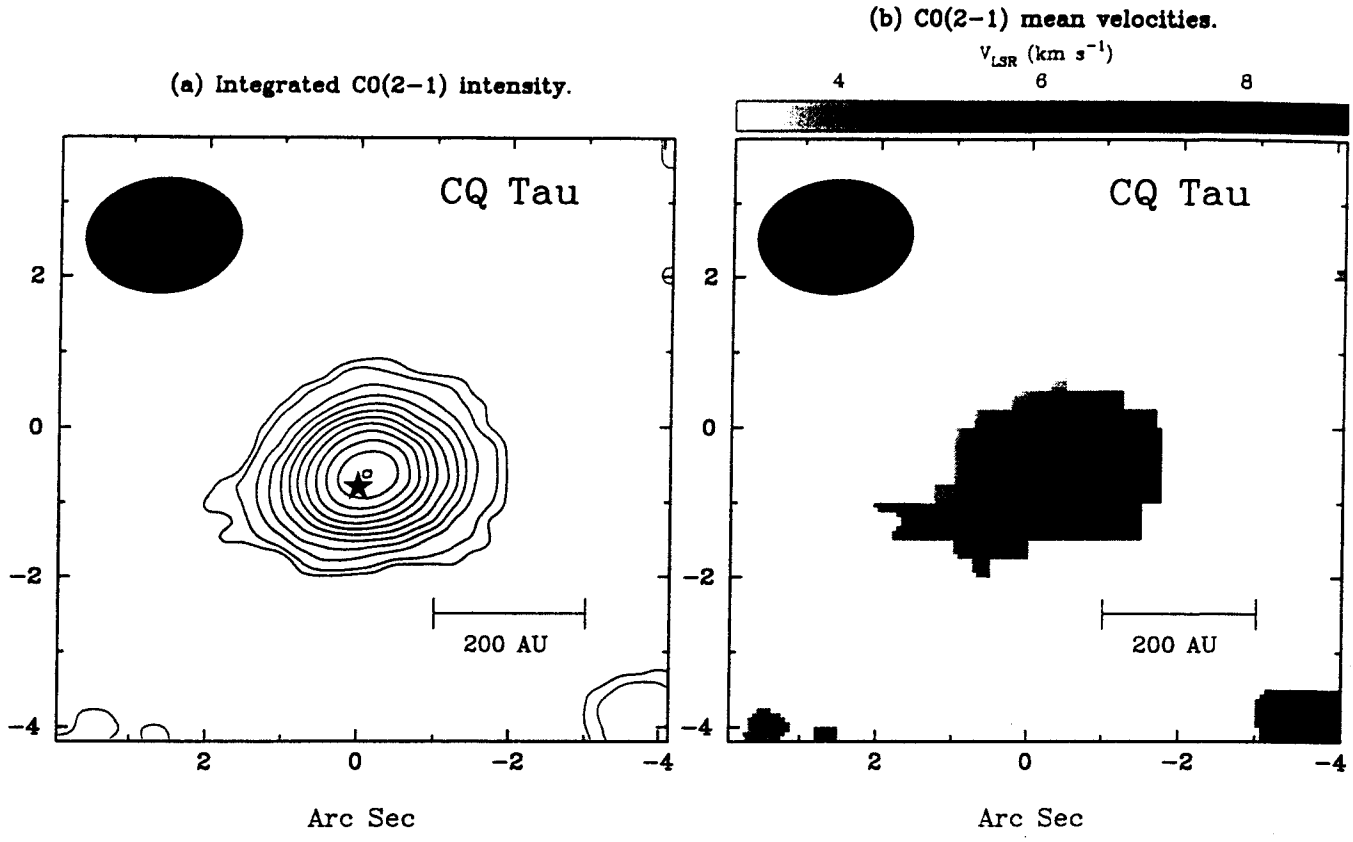

Fig. 3 (CONTINUED)

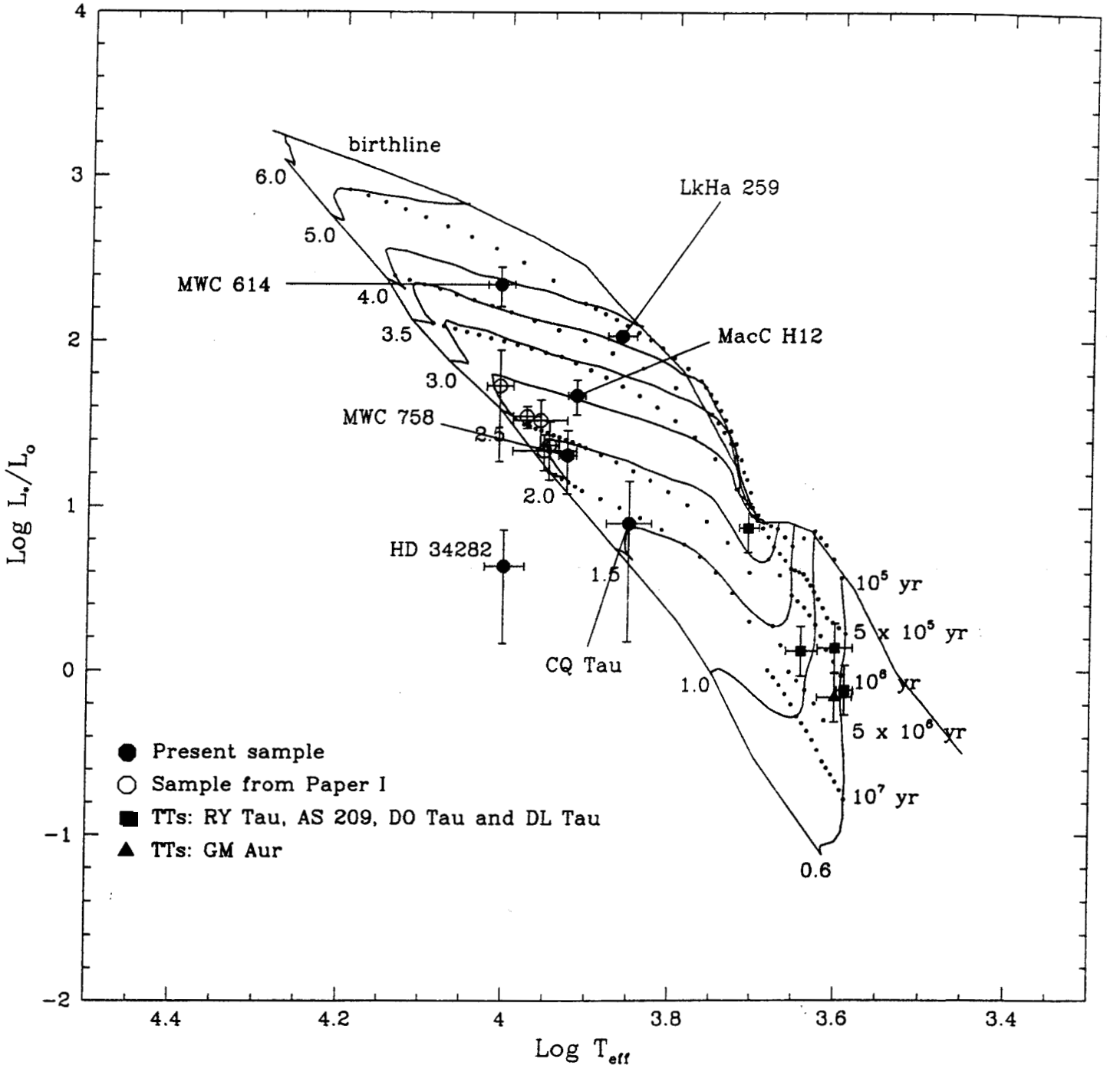
birthline
6.0
5.0
4.0
3.5
3.0
2.5
2.0
1.5
1.0
0.6
LkHa 259
MacC H12
MWC 614
MWC 758
HD 34282
CQ Tau
10^5 yr
5 x 10^5 yr
10^6 yr
5 x 10^6 yr
10^7 yr
Present sample
Sample from Paper I
TTs: RY Tau, AS 209, DO Tau and DL Tau
TTs: GM Aur
Log $L_*/L_\odot$
Log T_{eff}
4
3
2
1
0
−1
−2
4.4
4.2
4
3.8
3.6
3.4

Fig.4

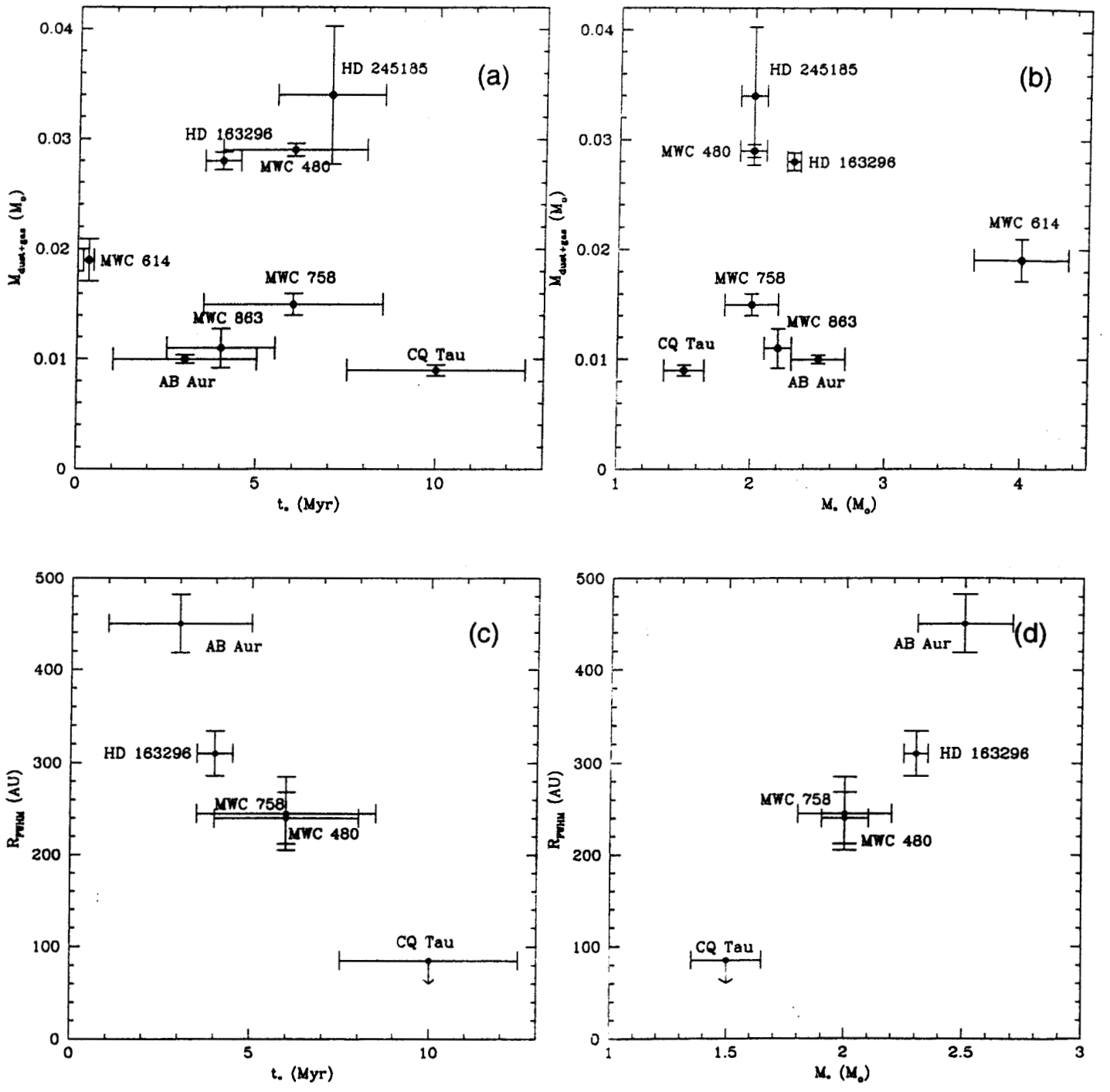
(a)
HD 245185
HD 163296
MWC 480
MWC 614
MWC 758
MWC 863
AB Aur
CQ Tau
$M_{dust+gas}$ ($M_\odot$)
t_* (Myr)
(b)
HD 245185
MWC 480
HD 163296
MWC 614
MWC 758
MWC 863
CQ Tau
AB Aur
$M_{dust+gas}$ ($M_\odot$)
M_* ($M_\odot$)
(c)
AB Aur
HD 163296
MWC 758
MWC 480
CQ Tau
R_{FWHM} (AU)
t_* (Myr)
(d)
AB Aur
HD 163296
MWC 758
MWC 480
CQ Tau
R_{FWHM} (AU)
M_* ($M_\odot$)

Fig. 5

TABLE 1

SOURCE PARAMETERS.

(1) Star	(2) RA(1950)	(3) Dec(1950)	(4) Spectral Type[a]	(5) d (pc)	(6) $F_{1.3mm}$ (mJy)	(7) α_{submm}[b]	(8) A_V	(9) T_{eff}[c] (K)	(10) R_*[c] ($R_\odot$)	(11) L_*[c] ($L_\odot$)	(12) M_*[c] ($M_\odot$)	(13) Age[c] (Myr)
MWC 614	19[d]08 55.42	+15 42 15.1	B9/A0/IV/Ve	240^{+70}_{-40}[e]	...	...	1.27[e]	10220	4.7	221.9	4	0.3
HD 34282	05[d]13 38.09	−09 51 51.6	A0Ve+sh	160^{+60}_{-40}[e]	183[f]± 17	2.2[f]± 0.2	0.59[e]	10040	0.6	4.3	...	...
MWC 758	05[d]27 22.46	+25 17 42.9	A3e	200^{+60}_{-40}[e]	72[b]± 13	2.80[b]± 0.21	0.22[e]	8465	2.1	20.6	2	6
MacC H12	00[g]04 25.22	+65 21 56.9	A5/F:e	845[h]	44[h]± 5	...	5.55[h]	8270	3.0	47.1	2.5	3
CQ Tau	05[d]32 54.13	+24 43 03.9	A8V/F2IVe	100^{+25}_{-17}[e]	221[b]± 40	1.98[b]± 0.20	0.96[e]	7130	1.9	8.0	1.5	10
LkHα 259	23[i]56 09.60	+66 09 32.0	A9e	850	...	...	5.22[j]	7320	6.5	107.3	3.5	0.3

[a]Thé, de Winter & Pérez (1994).

[b]Mannings et al., in preparation.

[c]See §5, this work. Values of T_{eff}, R_* and L_* for MWC 758 and CQ Tau are from Paper I.

[d]Hipparcos and Tycho Catalogues (ESA 1997).

[e]van den Ancker, de Winter & Tjin A Djie (1998).

[f]Flux density at $\lambda = 1.1$ mm; from Sylvester et al. (1996).

[g]Herbig & Bell (1988).

[h]Osterloh & Beckwith (1995).

[i]Levrault (1988).

[j]See §2, this work.

TABLE 2

CONTINUUM MEASUREMENTS, AND DETERMINED QUANTITIES

(1) Source	(2) λ (mm)	(3) F_ν (mJy)	(4) $R_{\rm FWHM}$ (AU)	(5) $M_{\rm dust+gas}$[a] ($M_\odot$)	(6) $A_V(s{=}0)$[b]	(7) $A_V(s{=}\frac{3}{2})$[c]
MWC 614	2.6	7.6 ± 1.4	<450	0.015	...	...
MWC 614	1.3	70.8 ± 7.0	<230	0.019	19	403
HD 34282	2.6	23.8 ± 3.0	<270	0.021	24	483
MWC 758	1.3	82.5 ± 5.5	<185	0.015	188	$>10^3$
MacC H12	2.6	10.0 ± 1.4	<1625	0.234	17	698
CQ Tau	1.3	143 ± 8.4	<80	0.009	253	$>10^3$
LkHα 259	2.6	<6[d]	...	<0.142	...	...

[a]Assuming a gas-to-dust ratio of 100, by mass.

[b]As in Paper I, we adopt a power law form for the radial density profile, $\rho(r) \propto (r_o/r)^s$. Here, we consider a uniform density spherical envelope, of inner radius 1 AU.

[c]Freely-falling spherical envelope, of inner radius 1 AU.

[d]3σ upper limit.

TABLE 3

MOLECULAR LINE MEASUREMENTS, AND DETERMINED QUANTITIES

(1) Source	(2) Line	(3) v_0 (LSR) (km s^{-1})	(4) Δv (LSR)[a] (km s^{-1})	(5) $\int S_\nu dv$ (Jy km s^{-1})	(6) $R_{\rm FWHM}$ (AU)	(7) P.A. (deg.)	(8) i (deg.)	(9) $M_{\rm H_2}$ ($M_\odot$)
MWC 614	CO(1→0)	...	...	<0.279[b]	...	...	...	...
HD 34282	CO(1→0)	...	...	<0.486[b]	...	...	...	...
MWC 758	CO(2→1)	+5.9	+4.2 to +7.5	10.8	245 × 170	116^{+6}_{-5}	46	3.97×10^{-5}
MacC H12	CO(1→0)	−4.7	−2.1 to −7.3	49.5	4250 × 2870	136^{+3}_{-3}	48	3.64×10^{-2}
CQ Tau	CO(2→1)	+5.9	+2.9 to +10.1	32.3	<85	−	−	2.62×10^{-5}
LkHα 259	CO(1→0)	...	...	<0.256[b]	...	...	...	...

[a]Full width of line for which emission is above the 3-σ level.

[b]Upper limit, per beam, at 3σ across a channel of width 1.3 km s^{-1}

TABLE 4

COMPARISON OF AE DISK PROPERTIES WITH TTS DISKS

	Average Mass (gas+dust) ($M_\odot$)	Mass range ($M_\odot$)	Radii of dust components (AU)	Radii of molecular gas components (AU)
Ae systems[a]	0.020	0.009 – 0.034	$\lesssim 300$	85 – 450
T Tauri systems	0.010[b]	0.001 – 0.038[b]	≤ 180[c]	110 – 350[c]

[a]Sources are from Paper I and the present work. MacC H12 is excluded.
[b]Using 1.3-mm flux densities from Beckwith et al. (1990): see Paper I.
[c]From results of Koerner & Sargent (1995).